Ultrafast Events in the Folding of Ferrocytochrome *c*†

Rajesh Kumar, N. Prakash Prabhu, and Abani K. Bhuyan*

School of Chemistry, University of Hyderabad, Hyderabad 500046, India

Received March 1, 2005; Revised Manuscript Received April 14, 2005

ABSTRACT: Laser flash photolysis and stopped-flow methods have been used to study the dynamic events in the micro- to millisecond time bin in the refolding of horse ferrocytochrome *c* in the full range of guanidine hydrochloride concentration at pH 12.8 (±0.1), 22 °C. Under the absolute refolding condition, the earliest relaxation time of the unfolded protein chain is less than 1 μs. The chain then undergoes diffusive dynamics-mediated contraction and expansion, in which intrapolypeptide ligands make transient contacts with the heme iron, giving rise to two distinct kinetic phases of ∼0.4 and ∼3 μs. Under moderate to absolute refolding conditions, the rates of these processes show little dependence on the denaturant concentration, indicating the absence of structural element in the incipient or the relaxed state. Chain expansion and contraction events continue until the polypeptide finds a stable and supportive transition state. The crossing of this transition barrier, which rate-limits the folding of alkaline ferrocytochrome *c*, is characterized by a stopped-flow measured time constant of ∼3 ms in aqueous solvent. Observed kinetics thus implicate no submillisecond folding structure. The folding kinetics is effectively two state in which the unfolded polypeptide first relaxes to an unstructured chain and then crosses over a late rate-limiting barrier to achieve the native conformation. The experimentally observed rates as a function of guanidine hydrochloride concentration have been simulated by numerically calculated microscopic rates of a simple kinetic model that captures the essential features of folding.

Isolated peptide fragments in solution often show a tendency to form helices and turns (*1*−*3*), and they may form too rapidly in the intact protein. For example, folding of the model peptide α-helix (*4*−*6*) and β-hairpin fragment (*7*) occurs in nanoseconds to a few microseconds. These observations raise the possibility that small single-domain proteins could also have submillisecond folding phases in which secondary structural elements are seeded for facilitating efficient and biased folding. Fast folding experiments have thus attracted the attention of many for over a decade.

The first ultrafast experiment was based on the fact that the two-state folding transition (N ⇌ U) of ferrocytochrome *c* (ferrocyt *c*) is shifted to a lower concentration of guanidine hydrochloride (GdnHCl)[1] when the solvent is saturated with ∼1 mM CO (*8*, *9*). The shift occurs because of preferential binding of CO to the unfolded protein. Within a narrow range of GdnHCl, between ∼4.2 and 4.7 M, the CO-bound protein is unfolded, but the CO-free form is nativelike. It follows that photodissociation of CO within this window of GdnHCl will initiate folding (*8*). However, this is an extremely poor condition to study protein folding, since the required concentration of the denaturant to make the experiment work is just too close to the transition midpoint (∼5.1 M GdnHCl) of ferrocyt *c* (*9*). A similar photochemical protocol that takes advantage of the stability difference of the two oxidation states of cyt *c* in order to initiate refolding of ferrocyt *c* by rapidly injecting an electron into the ferric heme of unfolded ferricyt *c* (*10*) works only under conditions where no substantial driving force for folding is available.

In other approaches, laser T-jump methods have been used to monitor fast folding events for a number of peptides and proteins, including barstar (*11*), apomyoglobin (*12*−*14*), EnHD protein (*15*), and λ_{6-85} protein (*16*). An elegant application of laser flash photolysis for direct estimation of the speed limit for protein folding has been described (*17*). Ultrarapid mixing methods have been introduced to measure the earliest folding events in ferricyt *c* (*18*−*21*), acyl-CoA binding protein (*22*), the four-helix protein Im7 (*23*), and β-lactoglobulin (*24*). NMR and hydrogen-exchange methods have been used for microsecond studies of monomeric λ repressor (*25*) and a crossed-link variant of the GCN4 coiled coil (*26*).

For several reasons, however, carbonmonoxy-cyt *c* continues to be an indispensable standard system in the fast-folding field. Being a single-domain fast-folding protein, ferrocyt *c* is paradigmatic (*9*, *27*−*30*). Since photodissociation of CO occurs in subpicosecond times (*31*), there is virtually no dead time in probing the dynamics of the refolding polypeptide. The presence of the heme renders possible the use of a variety of additional spectroscopic probes in the time-resolved mode, including optical spectroscopy and magnetic circular dichroism (*32*, *33*). Even

† This work was supported by grants from the Department of Biotechnology (BRB/15/227/2001) and the Department of Science and Technology (4/1/2003-SF) and by the University Grants Commission (UPE Funding), Government of India. A.K.B. is the recipient of a Swarnajayanti Fellowship from the Department of Science and Technology.

* To whom correspondence should be addressed. E-mail: akbsc@uohyd.ernet.in. Phone: 91-40-2313-4810. Fax: 91-40-2301-2460.

[1] Abbreviations: GdnHCl, guanidine hydrochloride; cyt *c*, cytochrome *c*; ferricyt *c*, ferricytochrome *c*; ferrocyt *c*, ferrocytochrome *c*; carbonmonoxy-cyt *c*, carbon monoxide-bound ferrocytochrome *c*; TOF, time of flight; ΔG_D, Gibbs energy of denaturation; $\Delta G_D°$, Gibbs energy of denaturation in the absence of denaturant.

10.1021/bi050384b CCC: $30.25 © 2005 American Chemical Society
Published on Web 06/10/2005

though low denaturant conditions under which CO photolysis could generate a large driving force to folding were not found in earlier studies, the carbonmonoxy-cyt *c* system has been used extensively to extract information about diffusive dynamics of polypeptides in solvents containing denaturing to unfolding concentrations (4−7.4 M) of GdnHCl (*34*, *35*).

We have now found absolute refolding conditions under which CO photolysis can be performed to check for ultrafast events in the folding of ferrocyt *c*. In strongly alkaline medium CO-bound ferrocyt *c* is steadily unfolded irrespective of the inclusion or exclusion of GdnHCl. On the other hand, NMR spectra indicate that, in the absence of CO and GdnHCl, alkaline ferrocyt *c* is very similar to the neutral pH native state in terms of secondary and tertiary structural content (*30*). Alkaline ferrocyt *c* exhibits a well-defined cooperative unfolding transition when titrated with GdnHCl ($C_m \approx 2.6 \pm 0.2$ M). On the basis of these observations, we have poised carbonmonoxy-cyt *c* for laser photolysis in the 0−4 M range of GdnHCl. The results in conjunction with millisecond stopped-flow data have been used to present a two-state folding model. Observed rates in micro- to millisecond times have been numerically simulated by calculations of microscopic rates. Submillisecond events in the folding of alkaline ferrocyt *c* consist of an initial relaxation followed by rapid contraction and expansion of the chain until a rate-limiting folding barrier is found.

MATERIALS AND METHODS

Equine cyt *c* (type VI), GdnHCl, and sodium dithionite were from Sigma, USB, and Merck, respectively. Experiments were done in strictly anaerobic atmosphere at 22 °C, pH 12.7−13.0, using NaOH with or without 1−2 mM CAPS [3-(cyclohexylamino)-1-propanesulfonic acid]. Solutions contained 0.5−3 mM freshly prepared sodium dithionite, and experiments were completed within 2 h of exposing the protein to high pH. Fluorescence changes at high pH were corrected by using NATA fluorescence.

Equilibrium Unfolding. Cyt *c* solutions, with or without 1 mM CO, were deaerated and reduced under nitrogen with 1 mM sodium dithionite and incubated in tightly capped quartz cuvettes or rubber-capped glass tubes for ∼30 min. Fluorescence emission spectra (excitation 280 nm) were taken in a FluoroMax-3 instrument (Jobin-Yvon, Horiba). Optical absorption spectra were recorded in a UV-3101PC (Shimadzu) or Cary 100 (Varian) spectrophotometer. Data were analyzed using the standard two-state equation for equilibrium unfolding (*36*) as described in earlier studies of ferrocyt *c* (*29*).

Stopped-Flow Measurements. All stopped-flow experiments involved two-syringe mixing. Cyt *c*, initially unfolded in ∼5 M GdnHCl and held at pH 12.7 by employing 2 mM CAPS and concentrated NaOH, was reduced under nitrogen by adding a concentrated solution of sodium dithionite to a final concentration of ∼3 mM and incubated at 22 °C for ∼30 min. The final protein concentration in the refolding mixture was in the 10−15 μM range. In unfolding experiments, performed following the same procedure of two-syringe mixing, the final protein concentration was 6−10 μM. Kinetics were measured using a SFM 400 mixing module (Biologic). The excitation wavelength was 280 nm, and emission was measured using a 335 nm cutoff filter. Typically, 10 shots were averaged. Traces were analyzed using single- or double-exponential functions to extract apparent rates, λ_i, the initial signal, S_0, that corresponds to the "zero-time" signal in the stopped-flow time window, the observed signal, S_{obs}, and the final equilibrium signal, S_∞, corresponding to the signal value at $t = t_\infty$. The S_0, S_{obs}, and S_∞ signals were subjected to initial normalization by first subtracting the buffer fluorescence signals and then dividing by the recorded signal of the unfolded protein in the highest GdnHCl concentration. In the unfolding set of measurements the S_∞ value of the kinetic trace at the highest concentration of GdnHCl employed was used to divide the fluorescence signals.

Laser Photolysis and Microsecond Measurements. Cyt *c* solutions (10−12 μM), prepared in 2 mM CAPS and concentrated NaOH, pH 12.9 (±0.1), were deaerated and reduced by the addition of 2 mM sodium dithionite and were incubated for 15−30 min at 22 °C under 1 atm of CO gas pressure in tightly capped 1 cm squared quartz cuvettes. CO photolysis was achieved by irradiation with 45 (±10) mJ pulses of the 532 nm second harmonic light of a Spectra Physics Q-switched Nd:YAG laser (10 Hz). Spectral changes following each photolysis pulse were recorded with a pulsed Xe lamp. The basic configuration of the instrument is based on the Applied Photophysics laser flash photolysis spectrometer. The sample temperature was maintained by using an external circulating water bath. Single-wavelength kinetic traces were analyzed by single- or double-exponential functions as described under Results.

Simulation of Kinetic Data. For numerical calculation of the microscopic rate constants, k_j (j = +M, −M, +H, −H, +CO, −CO, f, and u), a 5 × 5 rate matrix was set up from the five coupled linear differential equations for the states represented by Fe^{2+}, Fe^{2+}−Met, Fe^{2+}−His, Fe^{2+}−CO, and N. The eigenvalues, λ_i (i = 1 to 4), computed by diagonalizing the rate matrix are functions of k_js, the logarithms of which were assumed to have quadratic dependence on GdnHCl concentration according to the equation:

$$k_j = k_j^0 \exp\left[\frac{m^\ddagger_j[\mathrm{GdnHCl}] + m^\ddagger_j[\mathrm{GdnHCl}]^2}{RT}\right]$$

where k_j^0 is the value of k_j in the absence of GdnHCl and $m^\ddagger$ is related to the change in surface area. The apparent kinetic rates (i.e., stopped-flow observables) were thus simulated with calculated λ_i values by adjusting the k_j^0 and $m^\ddagger_j$ values as input parameters. In this type of modeling, numeric instability is often encountered as a result of overdetermination of some parameters. Satisfactory fits were, however, obtained by repetitive adjustment of parameters.

RESULTS

To set the rationale of submillisecond experiments, we first provide a set of basic results for ferrocyt *c* held near pH 12.8 (alkaline ferrocyt *c*). Several spectroscopic signatures show that the structures of alkaline and neutral pH ferrocyt *c* are largely similar (*30*). Further, TOF mass spectra and extensive ligand-binding experiments indicate no deamidation or aggregation at alkaline pH (data not shown). Figure 1a shows GdnHCl-induced unfolding of the protein at pH 12.7. Two-state analysis of the transition (*36*) yields a ΔG_D°

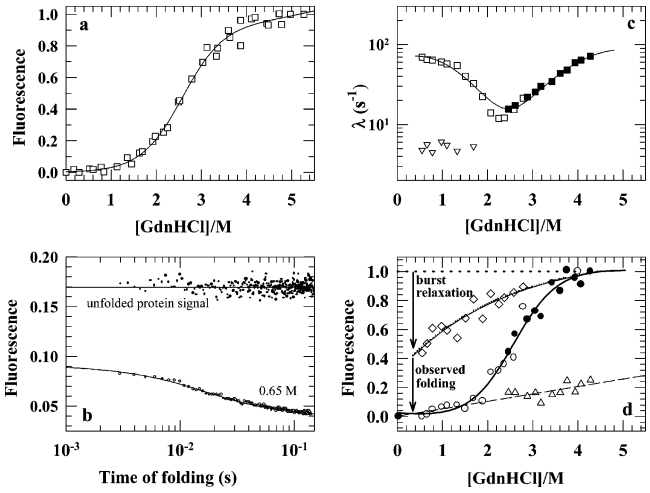

FIGURE 1: (a) GdnHCl unfolding of ferrocytochrome *c* at pH 12.7, 22 °C. Iterated fit values for a two-state equilibrium are $\Delta G_D^\circ \approx 3.5$ kcal mol^{-1}, and the equilibrium *m*-value, $m_g \approx 1.2$ (±0.1) kcal mol^{-1} M^{-1}. (b) The initial 140 ms of a representative stopped-flow kinetic trace for refolding in the presence of 0.65 M GdnHCl showing the recovery of the fluorescence signal, with respect to the fluorescence signal of the unfolded protein, during the burst kinetic phase. (c) GdnHCl dependence of rates for folding (□) and unfolding (■) under the same conditions of pH and temperature. (d) Normalized signal values at time $t = 0$ and $t = \infty$ (S_0 and S_∞, respectively) in folding and unfolding kinetics. Burst relaxation, shown by the upper arrow, refers to any stopped-flow unobservable submillisecond process that causes a loss of spectroscopic signals. GdnHCl dependence of S_0 values in refolding (◇) is empirically described by $y = a - b \exp(-cx)$, where *a*, *b*, and *c* are constants. S_0 values for unfolding (△) describe an extension of the native state baseline as a function of GdnHCl. The S_∞ signals recorded in refolding (○) and unfolding (●) experiments reproduce the equilibrium unfolding transition shown in panel a. The fit through these data also yields the same values of ΔG_D° and m_g.

value of 3.5 kcal mol^{-1}, and the equilibrium *m*-value $m_g \approx 1.2$ (±0.1) kcal mol^{-1} M^{-1}.

Figure 1b shows a stopped-flow trace for the refolding of alkaline ferrocyt *c* in the presence of 0.65 M GdnHCl, pH 12.7. The fluorescence signal recorded for the unfolded protein (~5 M GdnHCl, pH 12.7) is also plotted. Clearly, a major fraction of the signal (~55%) is already recovered within the dead time of the stopped flow, indicating the presence of a submillisecond relaxation process. This burst loss of signal has a strong dependence on the concentration of GdnHCl in the refolding buffer; the lower the final denaturant concentration, the larger the recovery. The observed refolding time courses were, in general, fitted to one exponential. In some cases two exponentials were needed to improve the overall quality of fits (Figure 1b). The slow minor phase, the amplitude of which averages to ~10% of the observed signal, represents most likely the fraction of the oxidized protein and was excluded from further analysis. Figure 1c shows GdnHCl dependence of the logarithm of the observed refolding (unfolding) rate. Within error, the minimum of this chevron matches the midpoint of the unfolding transition (Figure 1a). Under strongly refolding conditions the rates deviate away from linearity. The nonlinearity of folding chevrons is generally taken as an indication of fast accumulation of folding intermediates (*37*). Denaturant dependence of folding rates for ferricyt *c* has been analyzed by invoking structural intermediates (*20*, *38*), although this interpretation has been questioned (*39*). In the context of ferrocyt *c*, where interpretational ambiguities arising from heme misligation are removed, our earlier studies have shown that the nonlinear feature of the folding chevron is not due to accumulation of folding intermediates. Very recently, we have analyzed in detail the folding kinetics in the rollover region and found no evidence for accumulation of a kinetic intermediate (*29*). The observed nonlinearity may be due to reasons that include some structural changes of the folding transition state along the reaction coordinate (*40*) and rapid interconversion of different configurations of the initial chain ensemble in the time scale of their conversion to the native state (*41*). In this perspective, the GdnHCl dependence of the observed rates is fitted within the constraint of the two-state N ⇌ U model by assuming the ad hoc polynomial relationship between log $k_{f(u)}$ and GdnHCl (*40*):

$$\log k_{f(u)} = \log k_{f(u)}{}^0 + m_{1,f(u)}[D] + m_{2,f(u)}[D]^2$$

where $k_{f(u)}{}^0$ are folding and unfolding rate constants in water.

Figure 1d quantifies denaturant dependences of fluorescence signal amplitudes at times $t = 0$ and $t = \infty$ of folding and unfolding. The GdnHCl dependence of $t = \infty$ signals in both folding and unfolding kinetic traces, S_∞, reproduces the equilibrium unfolding transition (Figure 1a), and the thermodynamic parameters extracted from the two transitions are in excellent agreement. Of particular interest is the GdnHCl dependence of the fluorescence at $t = 0$ (S_0), normalized with reference to the fluorescence of the unfolded protein (Figure 1b). S_0 decreases as the GdnHCl concentration in the folding medium is lowered. The upper arrowhead in Figure 1d shows the unobservable fluorescence change associated with the stopped-flow burst phase. The lower arrowhead indicates the fluorescence observed in the millisecond folding regime.

The obvious inquiry that follows is what happens in the submillisecond burst phase. A common analysis, when submillisecond events have not been resolved in real time, involves the assumption that GdnHCl dependence of the S_0 values is the reminiscence of a distinct sigmoidal transition of a refolding intermediate that is fully formed within the dead time of stopped flow (refs *38* and *42*, for example). However, it is difficult to ascertain the exact functional dependence for GdnHCl vs S_0, given the practical limitation of obtaining relatively accurate burst phase data. The fit through the S_0 data in Figure 1d is an empirical one, and it does not appear to indicate a distinct denaturant-induced phase transition. One may still choose to interpret such a curve as a sigmoidal plot that is missing the pretransition, and thus the shape of the curve could simply reflect marginal stability of an intermediate. These difficulties make direct measurement of microsecond kinetics imperative.

In the present study, microsecond measurements entailed finding conditions that would facilitate ultrafast initiation of refolding by laser photolysis. We first describe how the system is poised for photolysis. Even though ferrocyt *c* in aqueous alkaline solution possesses structural integrity very similar to that at neutral pH, it readily denatures when CO is allowed to bind at pH >12. Notably, CO binding to alkaline ferrocyt *c* was described by Theorell and Åkesson some 60 years ago (*43*). By titrating the protein solution with CO at pH 12.8, we find that only one CO binds per molecule

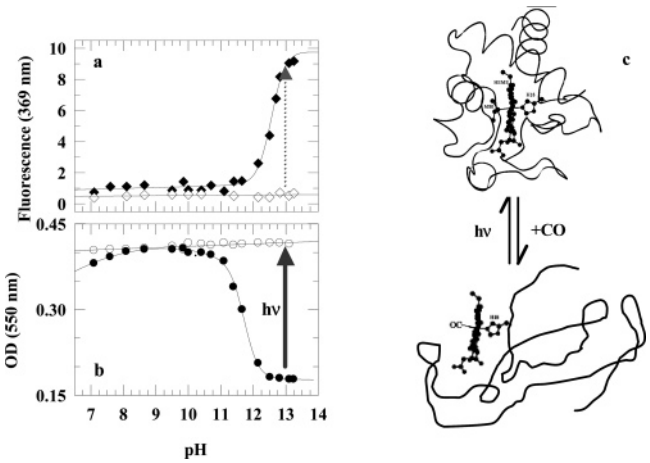

FIGURE 2: The basis of ultrafast initiation of folding. (a) Alkaline pH-induced unfolding of ferrocytochrome *c*. When CO is allowed to bind to the protein, it is fully unfolded at pH >12.8 (◆), but in the absence of CO there is no unfolding (◇). (b) The same transition is monitored by heme absorption (●). In the absence of CO the protein does not unfold (○). Because heme optical absorption is very sensitive to heme saturation by ligands, the CO-induced unfolding transition appears to shift to lower pH, relative to that measured by fluorescence, by ~0.5 unit. The arrow indicates that CO photolysis at a pH of ~12.8 initiates refolding. For convenience of kinetic measurements optical absorption spectroscopy was used to monitor postphotolysis events. (c) Schematic of the basis of photolysis-induced ultrafast folding. The CO-liganded protein is unfolded where the polypeptide is random. A light pulse dissociates CO and almost instantaneously initiates the folding reaction. Photolysis was carried out as a function of GdnHCl in order to derive a mechanistic description of folding (see also Figure 1).

of ferrocyt *c* with an equilibrium association constant, K_a, of $\sim 0.6 \times 10^6$ M^{-1} (data not shown). Figure 2a shows fluorescence-monitored pH titration curves of ferrocyt *c* in the presence and absence of 1 mM CO. In the absence of CO, the protein remains folded even at pH >13. The pH midpoint for unfolding in the presence of CO is ≈12.5. Figure 2b shows the same titration monitored by optical density at 550 nm. The results are same, except that the pH midpoint of the CO-induced unfolding transition appears at ~11.75. The shift may appear to indicate the accumulation of an equilibrium intermediate of ferrocyt *c* stabilized by CO (*44*), but it is not clear how the binding of an extrinsic gaseous ligand can do so. Also, observation of distinct transition curves of two different properties for the denaturation does not necessarily provide a proof of the existence of an intermediate (*45*). In any case, the observations recorded in Figure 2 imply that photolysis of CO will drive the protein to refold near pH 12.8 (indicated by an arrowhead in Figure 2b), and since CO photodissociation occurs in the subpicosecond regime, the folding course can be interrogated with virtually no time limitation (Figure 2c). Now, a comparison of Figures 1a and 2a,b shows that the CO photolysis method can be readily exploited to initiate ultrafast events in the folding of alkaline ferrocyt *c* in the full range of GdnHCl concentration.

CO photolysis was carried out in solutions of ferrocyt *c* liganded with CO in the presence of different concentrations of GdnHCl (0−4 M range), all held at pH 12.9 (±0.1), 22 °C. The microsecond relaxation processes thereafter are probed by absorption spectroscopy using a pulsed xenon lamp. Optical density is recorded at 421 nm, which is the λ_{max} in the difference spectrum of the folded protein in the

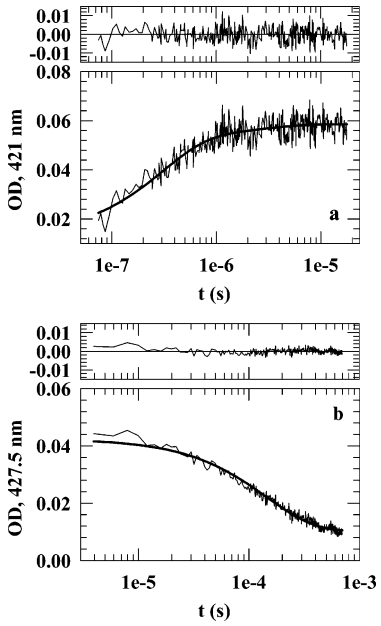

FIGURE 3: (a) Microsecond relaxation processes observed in heme optical absorption following photolysis of CO from carbonmonoxy-cyt *c* dissolved in ~1.5 mM CAPS containing 0.35 M GdnHCl, pH 12.9, 22 °C. The kinetics are described by two relaxations (residuals shown) of time constants ~0.32 and ~2.6 μs. (b) Bimolecular rebinding kinetics of CO illustrated for the F1−65 fragment of cytochrome *c* ($\tau \sim 160$ μs). To note is the much slower CO rebinding time (~750 μs) for the intact protein (see Figure 4).

absence of CO and the unfolded protein in the presence of CO. Figure 3a shows the observed changes in 421 nm absorption from 75 ns to 20 μs after CO photodissociation in the presence of 0.35 M GdnHCl. The data are best described by a two-exponential fit with relaxation times of $\tau_1 \sim 300$ ns and $\tau_2 \sim 2.5$ μs. After ~50 μs, the optical absorption starts to decrease slowly in a single-exponential decay time, $\tau_3 \sim 700$ (±300) μs. This is best illustrated for photolysis of CO in the heme−CO complex of the nonfolding fragment, F1−65, of cyt *c*, where the rate is faster (Figure 3b; $\tau \sim 200$ μs).

These three phases are detected consistently under all experimental conditions in the 0−4 M range of GdnHCl. The first phase and the second phase ($\tau_1 \sim 300$ ns and $\tau_2 \sim 2.5$ μs) are due to transient binding of methionines (M80 and M65) and histidines (H26 and H33), respectively, to the heme iron of the photoproduct that has already relaxed. We will use the symbol U′ for the relaxed photoproduct or the incipient chain. Note that H18 persists as one of the axial ligands of Fe^{2+} under all conditions. There could be a slight difference in the rates of binding of M80 and M65, and, similarly, for H26 and H33, because the binding rate depends on the number of amino acid residues that separate H18 and the binding residue. However, resolution of such a small difference in the relaxation profiles here is not expected. As such, τ_1 is assigned to transient binding of both methionines and τ_2 to both histidines. States corresponding to bound methionines and histidines will be symbolized $U'_{Fe^{2+}-Met}$ and $U'_{Fe^{2+}-His}$, respectively. These assignments are consistent with earlier studies on the rate of intrachain contact formation in unfolded ferrocyt *c* (*8*, *27*, *33*−*35*, *46*). More specifically, Hagen et al. (*35*) have used histidine mutants of cytochrome *c* to validate the assignments. We have also examined some aspects of the assignments by photolysis of the CO complex

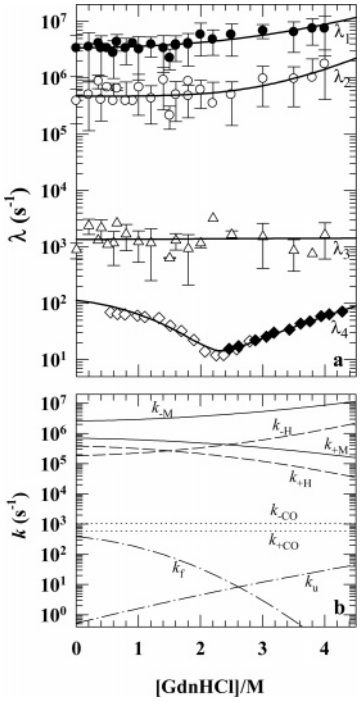

FIGURE 4: (a) GdnHCl dependence of the four observable rates in the folding of alkaline ferrocyt *c*. As described in the text, λ_1 (●) and λ_2 (○) correspond to the rates for binding of methionines and histidines, respectively. λ_3 (△) is assigned to CO rebinding. λ_4 are stopped-flow measured millisecond rates (◇, refolding; ◆, unfolding). The fits through the data are obtained from eigenvalue simulation of the folding model described in the text. (b) GdnHCl dependences of the microscopic rate constants, k_j, that constitute the eigenvalues, λ_i, according to the folding model.

Scheme 1

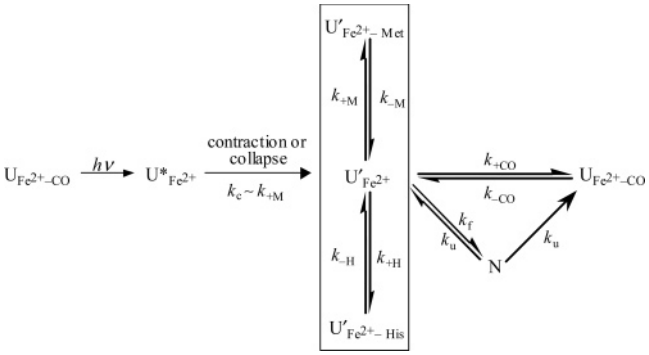

of one of the fragments of cyt *c* (F1−65) that excludes M80 (not shown). The slower third phase ($\tau_3 \sim 700\ \mu$s) is due to bimolecular rebinding of CO to the $U'_{Fe^{2+}}$ state. The rebinding reaction tends to obscure any relaxation process that may occur in a few hundreds of microseconds, because CO rebinding takes the $U'_{Fe^{2+}}$ polypeptide back to the initial unfolded state, $U_{Fe^{2+}-CO}$.

Altogether, there are four measurable relaxations in the folding of ferrocyt *c*: three are extracted from photolysis experiments and one from stopped-flow traces. Figure 4a shows how these relaxation rates vary with GdnHCl. To achieve a comprehensive description of the rate processes for the protein folding mechanism, the four measured relaxations (λ_1 to λ_4) can be considered within the framework of a phenomenological model shown in Scheme 1.

Various states and the processes indicated in the model are summarized briefly here. When photolyzed by a light pulse ($h\nu$), the unfolded CO-bound protein ($U_{Fe^{2+}-CO}$) goes to the high-energy unfolded state ($U^*_{Fe^{2+}}$). This happens nearly instantaneously. $U^*_{Fe^{2+}}$ has a vibrationally hot heme and an unrelaxed expanded polypeptide chain as observed in molecular dynamics simulation studies of cooling in laser-excited heme proteins including cyt *c* (ref *47*, for example). It then relaxes to a relatively unconstrained incipient state ($U'_{Fe^{2+}}$), the heme iron of which establishes transient contacts with methionines ($U'_{Fe^{2+}-Met}$) and histidines ($U'_{Fe^{2+}-His}$). The transient binding and dissociation events effectively produce a measurable distribution of three populations of the relaxed protein shown by the equilibria $U'_{Fe^{2+}-Met} \rightleftharpoons U'_{Fe^{2+}} \rightleftharpoons U'_{Fe^{2+}-His}$. The equilibria suggest that the incipient chain contracts and expands constantly, and the box enclosure indicates that the rates of contraction and expansion are much faster than the rate of its folding to the native state (N) or of unfolding to the equilibrium unfolded state ($U_{Fe^{2+}-CO}$), the latter by rebinding with CO. The N state, of course, unfolds to $U_{Fe^{2+}-CO}$, because even native cyt *c* binds CO under the experimental conditions employed. Under thermal conditions, the reverse reaction from $U_{Fe^{2+}-CO}$ to N is negligible. The essence of this scheme is consistent with models described in earlier photolysis studies (*8*, *33*, *34*).

We now examine the GdnHCl dependences of the four measurable relaxations in the folding of ferrocyt *c*. To do so, only five states in the model ($U'_{Fe^{2+}-Met}$, $U'_{Fe^{2+}}$, $U'_{Fe^{2+}-His}$, N, and $U_{Fe^{2+}-CO}$) corresponding to the four measured eigenvalues (λ_1 to λ_4) are considered. The earliest phase of relaxation of the photoproduct (i.e., $U^*_{Fe^{2+}} \rightarrow U'_{Fe^{2+}}$) is excluded, since the experiments presented here do not provide any direct information about this process. The eigenvalues were simulated by numerical calculation of microscopic rate constants, k_j ($j = +$M, $-$M, $+$H, $-$H, $+$CO, $-$CO, u, and f), as described under Materials and Methods. Figure 4a shows the GdnHCl dependences of λ_i extracted from one of the solutions of eigenvalue simulation, and Figure 4b shows the denaturant dependences of k_j that yield the solution.

The calculated values of k_{+M}, k_{-M}, k_{+H}, and k_{-H} are the rates of diffusion of the methionine (M80 and M65) and histidine (H26 and H33) side chains into and out of the heme iron site. As modeled earlier (*8*), binding of an intrapolypeptide ligand, say M, to the heme involves first diffusive motions of M at a rate k_+ to produce a heme−ligand contact loop, the two ends of which are provided by the side chains of H18, which persists as an axial ligand in the $U'_{Fe^{2+}}$, and M. As shown, the side chain of the contacting residue can now form a bond with the heme iron at a rate k_{+b} or diffuse away at a rate k_-:

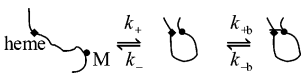

The overall rate of binding, k_{+M}, is given by

$$k_{+M} = k_+\left[\frac{k_{+b}}{(k_- + k_{+b})}\right]$$

Here $k_{+b} \gg k_-$, because the covalent binding, approximated by the geminate rate (tens of nanoseconds), occurs very rapidly compared to chain diffusion that takes microseconds.

Hence, $k_{+M} \approx k_{+}$. Thus, the calculated values of ligand contact rates are actually the diffusion rates.

As Figure 4b shows, under the absolute refolding condition achieved in the absence of GdnHCl, the diffusion rate of methionines is $k^0_{+M} \sim 2.6 \times 10^6$ s^{-1} ($\tau \sim 0.4$ μs). This is the fastest rate of chain contraction within the relaxed state, $U'_{Fe^{2+}}$. The relaxation rate of the polypeptide chain from the $U^*_{Fe^{2+}}$ to the $U'_{Fe^{2+}}$ state must therefore be greater than or equal to k^0_{+M}. Thus, the value of $\sim$0.4 μs presents an upper bound for the relaxation time of the immediate photoproduct. The rate of diffusive motions of histidine residues in the contact formation in aqueous solution, k^0_{+H}, is $\sim 2.8 \times 10^5$ s^{-1} ($\tau \sim 4$ μs).

Figure 4b also shows that the gradients of both k_{+M} and k_{+H} vs GdnHCl spaces are rather shallow in the subdenaturing limit (0−2 M GdnHCl). This observation has two implications. (i) Under strongly refolding conditions, the chain contraction events within the initial relaxed state are not associated with any substantial surface burial, implying little structure formation. (ii) The diffusive motions of the incipient polypeptide are only marginally affected under mild denaturing conditions. When strongly destabilizing conditions (>2 M GdnHCl) are employed, the chain contraction rates (k_{+M} and k_{+H}) become appreciably slower, due likely to the larger number of denaturant molecules bound to the polypeptide, and therefore slower internal diffusion (*34*).

The rate calculations presented here use a bimolecular form for CO rebinding. Figure 4b shows that the extracted rate for rebinding in the absence of GdnHCl, k^0_{+CO}, $\sim$ 600 s^{-1}, and the rate exhibits, within error, no dependence on GdnHCl concentration, indicating that the species that rebinds CO is little structured. However, the nonfoldable fragment, F1−65, of cyt *c* rebinds CO about 3-fold faster than the holoprotein does, indicating the influence of the full-length polypeptide in the rebinding reaction.

Since we carried out photolysis under the most strongly refolding conditions, the model must allow refolding of the U′ state to the native state. In these experiments, a refolding event that overlaps in time with the CO rebinding phase will be masked. No phase is, however, detected in the time window that straddles the chain contraction and CO rebinding phases. Further, as mentioned above, the photoproduct that rebinds CO is unstructured. These observations indicate the absence of refolding events of a few hundreds of microseconds. To achieve a complete description of the folding mechanism though, the model is simulated with millisecond stopped-flow rates, λ_4. As Figure 4b shows, eigenvalue calculations yield a refolding rate of $k_f^0 \sim 380$ s^{-1} ($\tau \sim 2.6$ ms) in the absence of GdnHCl. The corresponding unfolding rate is $k_u^0 \sim 0.52$ s^{-1} ($\tau \sim 1.9$ s).

DISCUSSION

The ability to carry out photolysis-initiated refolding in the entire range of GdnHCl concentration distinguishes this work from similar earlier studies that employed conditions under which folding could be initiated only within a narrow range of denaturant concentration near the transition midpoint, where the thermodynamic driving force for folding is not appreciable. The present results thus provide an opportunity to analyze the submillisecond folding events. The two general issues to address are what happens during the earliest events in the folding and whether a structural intermediate accumulates in the submillisecond course of folding.

The earliest event in the folding of many proteins is assumed to be a collapse or a compaction of the extended unfolded polypeptide in response to its placement under refolding conditions (*12*, *13*, *15*, *48*−*53*), although there have been difficulties in the understanding of the collapse time, the configuration and structural attribute of the collapsed chain, and the role of the collapsed species in efficient folding. The collapse time may be as fast as 0.25−20 μs, shown for apomyoglobin (*12*, *13*), slow in the millisecond domain, exemplified by the folding of bovine β-lactoglobulin (*52*), or much slower into several seconds, as documented for protein L (*53*). From the photolysis experiments we could not derive any clear information about the chain collapse in ferrocyt *c*. On the other hand, we cannot rule out the occurrence of this event. If one has to dwell on chain collapse, then, within the limit of our model, the $U^*_{Fe^{2+}} \rightarrow U'_{Fe^{2+}}$ relaxation must be implicated. The upper limit of $\sim$0.4 μs projected for this process is then the collapse time. Such a rapid submicrosecond collapse, where the radius of gyration presumably shifts toward a relatively compact state, is predicted by an analytical approach of homopolymer dynamics (*54*, *55*), although the predicted time slows down severalfold when hydrodynamic interactions are taken into account (*55*). However, given the empirical distribution of collapse time and rather complicated nature of heteropolymer collapse, there does not appear to be a simple approach to estimate the initial collapse time in protein folding.

What is the lifetime of the relaxed chain after photolysis? A number of our earlier studies have shown that the folding of ferrocyt *c* is a two-state process, but with a finite lifetime of the condensed chain (*27*−*30*). Within the resolution of the present experiments, the results show no folding process in the microsecond bin (Figure 4), implying a lasting lifetime of this species during which the chain undergoes rapid interconversion between different chain configurations. In optical absorption-probed photolysis experiments, the sensitivity of the Soret band to heme ligation facilitates detection of three such configurational subpopulations. But, it is clear that diffusive intrachain dynamics, not necessarily related to heme ligation, can generate a sizable set of chain configurations existing in equilibrium. In this picture, the initial photoproduct undergoes loop-mediated rapid contraction and expansion involving variable-length chain segments. The denaturant-dependent redistribution of the set of chain configurations may also contribute to the rollover of stopped-flow rates (Figures 1b and 4a; see ref *41*). For an ideal two-state protein, where only the unfolded and native states are considered, the initial chain condensation and transition state barrier crossing may be so tightly coupled that both chain relaxation and native structure formation are recovered in the same kinetic step. In such a case, chain relaxation and rate-limiting barrier crossings are concomitant (*26*, *53*), allowing virtually no lifetime to the relaxed state.

The denaturant dependence of expansion and contraction dynamics of the incipient state, $U'_{Fe^{2+}}$ (Figure 4), provides some insight to an apparently contentious issue: what role the initial relaxation plays toward efficient folding. It has been suggested that the earliest chain relaxation (or collapse) is generally "specific", meaning that the unfolded polypeptide

condenses specifically to a compact structure bearing nativelike intrachain contacts (*20*, *56*, *57*). In other words, the chain condenses in a deterministic manner to an early kinetic intermediate with nativelike secondary structure. Implicit to the specific process is a drastic reduction in the conformational space to be searched for folding. On the other hand, the relaxation could be "nonspecific", meaning that the chain merely condenses to a random configuration in response to its transfer from a strongly unfolding to a strongly refolding solvent. The nonspecifically condensed or relaxed state is just the unfolded state in a refolding environment (*28*−*30*, *39*, *51*, *58*−*61*). The postphotolysis dynamics of the ferrocyt chain, modeled by $U'_{Fe^{2+}-Met} \rightleftharpoons U'_{Fe^{2+}} \rightleftharpoons U'_{Fe^{2+}-His}$ equilibria, are conserved throughout the GdnHCl range (Figure 4). More importantly, the pertinent rate coefficients show little variation in the range of GdnHCl concentrations corresponding to the folding arm of the rate-denaturant space, indicating that the initial chain relaxation is nonspecific. Two lines of earlier evidence also lend support to the suggestion that it cannot be specific. (i) In stopped-flow denaturant dilution experiments, both nonfolding fragments of the protein (F1−65 and F1−80) and the normally refoldable holoprotein produce a quantitatively indistinguishable submillisecond signal at all concentrations of GdnHCl (*39*, *58*). This is true for the nonfolding holoprotein as well. Cyt *c* can be held under conditions that are persistently unfolding in the full range of GdnHCl or urea concentrations. In denaturant dilution experiments, even the unfolded protein shows submillisecond signals, the denaturant dependence of which matches that for the normal refolding protein (*29*). (ii) A recent laser T-jump study has found similar dynamics in the fast reconfigurations of the foldable holocytochrome *c* and its nonfolding fragments (*62*). In all cases, cytochrome *c* and its fragments both respond to solvent changes through the same relaxation.

Nonspecific contraction is expected to be significantly faster than the specific collapse. Indeed, we project $U^*_{Fe^{2+}} \rightarrow U'_{Fe^{2+}}$ relaxation to ∼0.4 μs, at least 100-fold faster than the value measured by Shastry and Roder for ferricytochrome *c* (*20*). Temperature-dependent activation of chain condensation is often associated with specificity (*20*), but simple chain contraction also meets with enthalpic barrier (see ref *61*).

To achieve forward folding, the nonspecifically contracted chain must find a viable and rate-limiting transition state. The photolysis results in conjunction with stopped-flow data show that the initial relaxation time of unfolded ferrocyt *c* is of the order ∼0.4−1 μs, and the observed folding time is in milliseconds (Figure 4). These results indicate that it is the transition of the relaxed state, U′, to the native state, N ($U' \rightarrow \ddagger \rightarrow N$), that sets the folding time. For kinetically two-state proteins such as ferrocyt *c* (*27*−*29*) and Csp B (*63*), where postbarrier kinetic intermediates do not accumulate, folding from the transition state to the native state ($\ddagger \rightarrow N$) is rapid and downhill biased. These considerations imply that almost the entire length of the observed folding time is the time needed for the U′ state to find a rate-limiting transition state. Although a general mechanism of how the transition state is found is not clear, it is suggested that the incipient chain is engaged in an energetically uphill search (*28*−*30*, *39*, *60*, *61*). The search continues until a relatively low-energy transition state conducive to forward folding is found. Because of the search−find approach, achieving the transition state is generally a time-consuming process. Experiments indicate an early transition state for cyt *c* (*28*, *29*, *64*) where at the most a third of the protein surface that is buried in the native state becomes buried (*28*). For the stopped-flow data presented in Figures 1 and 4, the surface burial in the transition state is much less than 30% of the buried area in the native state, implying that the folding transition state is more unfolded-like (see ref *30*). Experiments also indicate that the rate-limiting barrier is energetically sizable (*28*), ∼14 k_BT in the case of alkaline ferrocyt *c* (*30*). The transition state would thus appear modestly supported and stabilized by a few correctly formed nativelike tertiary contacts or long-range interactions. It is therefore dynamic and less organized, consistent with the observation that the folding transition state is more unfolded-like. This classical picture, definitely in contrast with the theoretical paradigm (see refs *65*−*69* and references cited therein), bears the essence of the topology search model (*28*, *39*, *70*, *71*) and is consistent with observations that folding rates and mechanisms often appear to be largely determined by the native state topology or contact order (*72*−*74*).

Finally, we comment on whether the spectroscopic probe used here is deficient for the detection of submillisecond structure formation. It may not appear so, because stopped-flow refolding chevrons of ferrocytochrome *c* measured by Soret heme absorbance, fluorescence, and far-UV CD are superimposable (*27*). Nevertheless, ultrafast CD studies of Kliger and co-workers (*33*, *75*), carried out in the presence of denaturing concentrations of GdnHCl, have reported on the submillisecond recovery of a minor fraction of the far-UV ellipticity value of native ferrocytochrome *c*. In view of this, it would be interesting to examine the postphotolysis events by time-resolved fluorescence (in progress) and CD under the present experimental conditions.

To conclude, we have described a simple experimental system of alkaline carbonmonoxy-cyt *c* that can be used for ultrafast protein folding studies under the absolute refolding condition. In this initial study, the Soret heme probe indicates that the refolding of alkaline ferrocyt *c* is kinetically a two-state process with no apparent involvement of structural intermediate. Upon initiation of refolding, the unfolded chain relaxes to an unstructured state of incipient chain. Mediated by intrapolypeptide diffusion, the relaxed chain undergoes continuous expansion and contraction in microsecond times until a stable rate-limiting transition state is found. The transition barrier crossing, and therefore rate-limited folding, is a late event occurring at a time of ∼3 ms.

ACKNOWLEDGMENT

We gratefully acknowledge helpful comments and criticisms by Walter Englander.

REFERENCES

1. Waltho, J. P., Feher, V. A., Merutka, G., Dyson, H. J., and Wright, P. E. (1993) Peptide models of protein folding initiation sites. 1. Secondary structure formation by peptides corresponding to the G- and H-helices of myoglobin, *Biochemistry 32*, 6337−6347.
2. Shin, H.-C., Merutka, G., Waltho, J. P., Wright, P. E., and Dyson, H. J. (1993) Peptide models of protein folding initiation sites. 2. The G-H turn region of myoglobin acts as a helix stop signal, *Biochemistry 32*, 6348−6355.
3. Shin, H.-C., Merutka, G., Waltho, J. P., Tennant, L. L., Dyson, H. J., and Wright, P. E. (1993) Peptide models of protein folding

initiation sites. 3. The G-H helical hairpin of myoglobin, *Biochemistry 32*, 6356−6364.
4. Williams, S., Causgrove, T. P., Gilmanshin, R., Fang, K. S., Callender, R. H., Woodruff, W. H., and Dyer, R. B. (1996) Fast events in protein folding: helix melting and formation in a small peptide, *Biochemistry 35*, 691−697.
5. Lednev, I. K., Karnoup, A. S., Sparrow, M. C., and Asher, S. A. (1999) α-helix peptide folding and unfolding activation barriers: a nanosecond UV resonance Raman study, *J. Am. Chem. Soc. 121*, 8074−8086.
6. Thompson, P. A., Eaton, W. A., and Hofrichter, J. (1997) Laser temperature jump study of the helix-coil kinetics of an alanine peptide interpreted with a "kinetic zipper" model, *Biochemistry 36*, 9200−9210.
7. Eaton, W. A., Muñoz, V., Thompson, P. A., Henry, E. R., and Hofrichter, J. (1998) Kinetics and dynamics of loops, α-helices, *β*-hairpins, and fast-folding proteins, *Acc. Chem. Res. 31*, 745−753.
8. Jones, C. M., Henry, E. R., Hu, Y., Chan, C. K., Luck, S., Bhuyan, A., Roder, H., Hofrichter, J., and Eaton, W. A. (1993) Fast events in protein folding initiated by nanosecond laser photolysis, *Proc. Natl. Acad. Sci. U.S.A. 90*, 11860−11864.
9. Bhuyan, A. K., and Kumar, R. (2002) Kinetic barriers to the folding of horse cytochrome *c* in the reduced state, *Biochemistry 41*, 12821−12834.
10. Pascher, T., Chesick, J. P., Winkler, J. R., and Gray, H. B. (1996) Protein folding triggered by electron transfer, *Science 271*, 1558−1560.
11. Nölting, B., Golbik, R., and Fersht, A. R. (1995) Submillisecond events in protein folding, *Proc. Natl. Acad. Sci. U.S.A. 92*, 10668−10672.
12. Ballew, R. M., Sabelko, J., and Gruebele, M. (1996) Observation of distinct nanosecond and microsecond protein folding events, *Nat. Struct. Biol. 3*, 923−926.
13. Ballew, R. M., Sabelko, J., and Gruebele, M. (1996) Direct observation of fast protein folding: the initial collapse of apomyoglobin, *Proc. Natl. Acad. Sci. U.S.A. 93*, 5759−5764.
14. Gilmanshin, R., Williams, S., Callender, R. H., Woodruff, W. H., and Dyer, R. B. (1997) Fast events in protein folding: relaxation dynamics of secondary and tertiary structure in native apomyoglobin, *Proc. Natl. Acad. Sci. U.S.A. 94*, 3709−3713.
15. Mayor, U., Guydosh, N. R., Johnson, C. M., Grossman, J. G., Sato, S., Jas, G. S., Freund, S. M. V., Alonso, D. O. V., Daggett, V., and Fersht, A. R. (2003) The complete folding pathway of a protein from nanoseconds to microseconds, *Nature 421*, 863−867.
16. Yang, W. Y., and Gruebele, M. (2003) Folding at the speed limit, *Nature 423*, 193−197.
17. Bieri, O., Wirz, J., Hellrung, B., Schutkowski, M., Drewello, M., and Kiefhaber, T. (1999) The speed limit for protein folding measured by triplet−triplet energy transfer, *Proc. Natl. Acad. Sci. U.S.A. 96*, 9597−9601.
18. Takahashi, S., Yeh, S.-R., Das, T. K., Chan, C.-K., Gottfried, D. S., and Rousseau, D. L. (1997) Folding of cytochrome *c* initiated by submillisecond mixing, *Nat. Struct. Biol. 4*, 44−50.
19. Chan, C.-K., Hu, Y., Takahashi, S., Rousseau, D. L., Eaton, W. A., and Hofrichter, J. (1997) Submillisecond protein folding kinetics studied by ultrarapid mixing, *Proc. Natl. Acad. Sci. U.S.A., 94*, 1779−1784.
20. Shastry, M. C. R., and Roder, H. (1998) Evidence for barrier-limited protein folding kinetics on the microsecond time scale, *Nat. Struct. Biol. 5*, 385−392.
21. Akiyama, S., Takahashi, S., Ishimori, K., and Morishima, I. (2000) Stepwise formation of α-helices during cytochrome *c* folding, *Nat. Struct. Biol. 7*, 514−520.
22. Teilum, K., Maki, K., Kragelund, B. B., Poulsen, F. M., and Roder, H. (2002) Early kinetic intermediate in the folding of acyl-CoA binding protein detected by fluorescence labeling and ultrarapid mixing, *Proc. Natl. Acad. Sci. U.S.A. 99*, 9807−9812.
23. Capaldi, A. P., Shastry, M. C., Kleanthous, C., Roder, H., and Radford, S. E. (2001) Ultrarapid mixing experiments reveal that Im7 folds via an on-pathway intermediate, *Nat. Struct. Biol. 8*, 68−72.
24. Kuwata, K., Shastry, R., Cheng, H., Hoshino, M., Batt, C. A., Goto, Y., and Roder, H. (2001) Structural and kinetic characterization of early folding events in *β*-lactoglobulin, *Nat. Struct. Biol. 8*, 151−155.
25. Huang, G. S., and Oas, T. G. (1995) Submillisecond folding of monomeric *λ* repressor, *Proc. Natl. Acad. Sci. U.S.A. 92*, 6878−6882.
26. Meisner, W. K., and Sosnick, T. R. (2004) Barrier-limited, microsecond folding of a stable protein measured with hydrogen exchange: implications for downhill folding, *Proc. Natl. Acad. Sci. U.S.A. 101*, 15639−15644.
27. Bhuyan, A. K., and Udgaonkar, J. B. (2001) Folding of horse cytochrome *c* in the reduced state, *J. Mol. Biol. 312*, 1135−1160.
28. Prabhu, N. P., Kumar, R., and Bhuyan, A. K. (2004) Folding barrier in horse cytochrome *c*: support for a classical folding pathway, *J. Mol. Biol. 337*, 195−208.
29. Kumar, R., and Bhuyan, A. K. (2005) Two-state folding of horse ferrocytochrome *c*: analyses of linear free energy relationship, chevron curvature, and stopped-flow burst relaxation kinetics, *Biochemistry 44*, 3024−3033.
30. Bhuyan, A. K., Rao, D. K., and Prabhu, N. P. (2005) Protein folding in classical perspective: folding of horse cytochrome *c*, *Biochemistry 44*, 3034−3040.
31. Anfinrud, P. A., Han, C., and Hochstrasser, R. M. (1989) Direct observation of ligand dynamics in hemoglobin by subpicosecond infrared spectroscopy, *Proc. Natl. Acad. Sci. U.S.A. 86*, 8387−8391.
32. Chen, E., Wood, M. J., Fink, A. L., and Kliger, D. S. (1998) Time-resolved circular dichroism studies of protein folding intermediates of cytochrome *c*, *Biochemistry 37*, 5589−5598.
33. Goldbeck, R. A., Thomas, Y. G., Chen, E., Esquerra, R. M., and Kliger, D. S. (1999) Multiple pathways on a protein-folding energy landscape: kinetic evidence, *Proc. Natl. Acad. Sci. U.S.A. 96*, 2782−2787.
34. Hagen, S. J., Carswell, C. W., and Sjolander, E. W. (2001) Rate of intrachain contact formation in an unfolded protein: temperature and denaturant effects, *J. Mol. Biol. 305*, 1161−1171.
35. Hagen S. J., Latypov, R. F., Dolgikh, D. A., and Roder, H. (2002) Rapid intrachain binding of histidine-26 and histidine-33 to heme in unfolded ferrocytochrome *c*, *Biochemistry 41*, 1372−1380.
36. Santoro, M. M., and Bolen, D. W. (1988) Unfolding free energy changes determined by the linear extrapolation method. Unfolding of phenylmethanesulfonyl alpha-chymotrypsin using different denaturants, *Biochemistry 27*, 8063−8068.
37. Sánchez, I. E., and Kiefhaber, T. (2003) Evidence for sequential barriers and obligatory intermediates in apparent two-state protein folding, *J. Mol. Biol. 325*, 367−376.
38. Colón, W., Elöve, G. A., Wakem, L. P., Sherman, F., and Roder, H. (1996) Side-chain packing of the N- and C-terminal helices plays a critical role in the kinetics of cytochrome *c* folding, *Biochemistry 35*, 5538−5549.
39. Sosnick, T. R., Mayne, L., and Englander, S. W. (1996) Molecular collapse: The rate limiting step in two-state cytochrome *c* folding, *Proteins 24*, 413−426.
40. Otzen, D. E., Kristensen, O., Proctor, M., and Oliveberg, M. (1999) Structural changes in the transition state of protein folding: alternative interpretations of curved chevron plots, *Biochemistry 38*, 6499−6511.
41. Parker, M. J., and Marqusee, S. (1999) The cooperativity of burst phase reactions explored, *J. Mol. Biol. 293*, 1195−1210.
42. Ikeguchi, M., Kuwajima, K., Mitani, M., and Sugai, S. (1986) Evidence for identity between the equilibrium unfolding intermediate and a transient folding intermediate: a comparative study of the folding reactions of alpha-lactalbumin and lysozyme, *Biochemistry 25*, 6965−6972.
43. Theorell, H., and Åkesson, A. (1941) Studies on cytochrome *c*. II. The optical properties of pure cytochrome *c* and some of its derivatives, *J. Am. Chem. Soc. 163*, 1812−1827.
44. Pabit, S. A., Roder, H., and Hagen, S. J. (2004) Internal friction controls the speed of protein folding from a compact configuration, *Biochemistry 43*, 12532−12538.
45. Dill, K. A., and Shortle, D. (1991) Denatured states of proteins, *Annu. Rev. Biochem. 60*, 795−825.
46. Hagen, S. J., Hofrichter, J., and Eaton, W. A. (1997) Rate of intrachain diffusion of unfolded cytochrome *c*, *J. Phys. Chem. B 101*, 2352−2365.
47. Henry, E. R., Eaton, W. A., and Hochstrasser, R. M. (1986) Molecular dynamics simulations of cooling in laser-excited heme proteins, *Proc. Natl. Acad. Sci. U.S.A. 83*, 8982−8986.
48. Agashe, V. R., Shastry, M. C., and Udgaonkar, J. B. (1995) Initial hydrophobic collapse in the folding of barstar, *Nature 377*, 754−757.

49. Chen, L., Wildegger, G., Kiefhaber, T., Hodgson, K. O., and Doniach, S. (1998) Kinetics of lysozyme refolding: structural characterization of a non-specifically collapsed state using time-resolved X-ray scattering, *J. Mol. Biol. 276*, 225−237.
50. Magg, C., and Schmid, F. X. (2004) Rapid collapse precedes the fast two-state folding of the cold shock protein, *J. Mol. Biol. 335*, 1309−1323.
51. Jacob, J., Krantz, B., Dothager, R. S., Thiyagarajan, P., and Sosnick, T. R. (2004) Early collapse is not an obligate step in protein folding, *J. Mol. Biol. 338*, 369−382.
52. Pollack, L., Tate, M. W., Finnefrock, A. C., Kalidas, C., Trotter, S., Dranton, N. C., Lurio, L., Austin, R. H., Batt, C. A., Gruner, S. M., and Mochrie, S. G. J. (2001) Time-resolved collapse of a folding protein observed with small-angle X-ray scattering, *Phys. Rev. Lett. 86*, 4962−4965.
53. Plaxco, K. W., Millett, I. S., Segel, D. J., Doniach, S., and Baker, D. (1999) Chain collapse can occur concomitantly with the rate-limiting step in protein folding, *Nat. Struct. Biol. 6*, 554−556.
54. Pitard, E., and Orland, H. (1998) Dynamics of the swelling or collapse of a homopolymer, *Europhys. Lett. 41*, 467−472.
55. Pitard, E. (1999) Influence of hydrodynamics on the dynamics of a homopolymer, *Eur. Phys. J. B 7*, 665−673.
56. Maki, K., Cheng, H., Dolgikh, D. A., Shastry, M. C., and Roder, H. (2004) Early events during folding of wild-type staphylococcal nuclease and a single-tryptophan variant studied by ultrarapid mixing, *J. Mol. Biol. 338*, 383−400.
57. Roder, H. (2004) Stepwise helix formation and chain compaction during protein folding, *Proc. Natl. Acad. Sci. U.S.A. 101*, 1793−1794.
58. Sosnick, T. R., Shtilerman, M. D., Mayne, L., and Englander, S. W. (1997) Ultrafast signals in protein folding and the polypeptide contracted state, *Proc. Natl. Acad. Sci. U.S.A. 94*, 8545−8550.
59. Qi, P. Q., Sosnick, T. R., and Englander, S. W. (1998) The burst phase in ribonuclease A folding: solvent dependence of the unfolded state, *Nat. Struct. Biol. 5*, 882−884.
60. Rumbley, J., Hoang, L., Mayne, L., and Englander, S. W. (2001) An amino acid code for protein folding, *Proc. Natl. Acad. Sci. U.S.A. 98*, 105−112.
61. Krantz, B. A., Mayne, L., Rumbley, J., Englander, S. W., and Sosnick, T. R. (2002) Fast and slow intermediate accumulation and the initial barrier mechanism in protein folding, *J. Mol. Biol. 234*, 359−371.
62. Qiu, L., Zachariah, C., and Hagen, S. J. (2003) Fast chain contraction during protein folding: "foldability" and collapse dynamics, *Phys. Rev. Lett. 90*, 168103.
63. Schindler, T., Herrler, M., Marahiel, M. A., and Schmid, F. X. (1995) Extremely rapid protein folding in the absence of intermediates, *Nat. Struct. Biol. 2*, 663−673.
64. Krishna, M. M. G., Lin, Y., Rumbley, J. N., and Englander, S. W. (2003) Cooperative omega loops in cytochrome *c*: role in folding and function, *J. Mol. Biol. 331*, 29−36.
65. Wolynes, P. G., Onuchic, J. N., and Thirumalai, D. (1995) Navigating the folding routes, *Science 267*, 1619−1620.
66. Dill, K. A., and Chan, H. S. (1997) From Levinthal to pathways to funnels, *Nat. Struct. Biol. 4*, 10−19.
67. Shakhnovich, E. I. (1997) Theoretical studies of protein-folding thermodynamics and kinetics, *Curr. Opin. Struct. Biol. 7*, 29−40.
68. Schonbrun, J., and Dill, K. A. (2003) Fast protein folding kinetics, *Proc. Natl. Acad. Sci. U.S.A. 100*, 12678−12682.
69. Onuchic, J. N., and Wolynes, P. G. (2004) Theory of protein folding, *Curr. Opin. Struct. Biol. 14*, 70−75.
70. Makarov, D. E., and Plaxco, K. W. (2003) The topomer search model: a simple, quantitative theory of two-state protein folding kinetics, *Protein Sci. 12*, 17−26.
71. Plaxco, K. W., Simons, K. T., and Baker, D. (1998) Contact order, transition state placement and the refolding rates of single domain proteins, *J. Mol. Biol. 277*, 985−994.
72. Baker, D. (2000) A surprising simplicity to protein folding, *Nature 405*, 39−42.
73. Plaxco, K. W., Simons, K. T., Ruczinski, I., and Baker, D. (2000) Topology, stability, sequence, and length: defining the determinants of two-state protein folding kinetics, *Biochemistry 39*, 11177−11183.
74. Bai, Y., Zhou, H., and Zhou, Y. (2004) Critical nucleation size in the folding of small apparently two-state proteins, *Protein Sci. 13*, 1173−1181.
75. Chen, E., Wittung-Stafshede, P., and Kliger, D. S. (1999) Far-UV time-resolved circular dichroism detection of electron-transfer-triggered cytochrome *c* folding, *J. Am. Chem. Soc. 121*, 3811−3817.

BI050384B